Uniqueness and Stability of Action Potential Models during Rest, Pacing, and Conduction Using Problem-Solving Environment

Leonid Livshitz and Yoram Rudy*
Cardiac Bioelectricity and Arrhythmia Center, Washington University in St. Louis, St. Louis, Missouri

ABSTRACT Development and application of physiologically detailed dynamic models of the action potential (AP) and Ca^{2+} cycling in cardiac cells is a rapidly growing aspect of computational cardiac electrophysiology. Given the large scale of the nonlinear system involved, questions were recently raised regarding reproducibility, numerical stability, and uniqueness of model solutions, as well as ability of the model to simulate AP propagation in multicellular configurations. To address these issues, we reexamined ventricular models of myocyte AP developed in our laboratory with the following results. 1), Recognizing that the model involves a system of differential-algebraic equations, a procedure is developed for estimating consistent initial conditions that insure uniqueness and stability of the solution. 2), Model parameters that can be used to modify these initial conditions according to experimental values are identified. 3), A convergence criterion for steady-state solution is defined based on tracking the incremental contribution of each ion species to the membrane voltage. 4), Singularities in state variable formulations are removed analytically. 5), A biphasic current stimulus is implemented to completely eliminate stimulus artifact during long-term pacing over a broad range of frequencies. 6), Using the AP computed based on 1–5 above, an efficient scheme is developed for computing propagation in multicellular models.

INTRODUCTION

Altered handling of intracellular Ca^{2+} and other regulatory molecules affects action potential (AP) generation and propagation and appears to play a central role in the development of cardiac arrhythmias (1). Regulation of intracellular molecular processes occurs over broad timescales. Although ion-channel activation and regulation of contraction by the binding of Ca^{2+} to contractile proteins are characterized by a fast timescale of response (micro- and milliseconds) (2), regulation by protein-kinase signaling networks (e.g., CaMKII, PKA) involves a longer timescale (seconds or minutes). In addition, slow rate-dependent accumulation of Ca^{2+} in the sarcoplasmic reticulum (SR) and Na^{+} in the myoplasm has an important inotropic effect in nonfailing myocytes and provides a foundation for the positive force-frequency relation in the normal heart (3,4). Depletion of intracellular and accumulation of extracellular K^{+} is well documented in both isolated single cell and tissue preparations during high level exercise, hypoxia or acidosis (5). These ionic processes influence the electrophysiological properties and propensity to arrhythmias; they require many beats (e.g., up to 30 min in canine atrial preparations (6) or in guinea-pig papillary muscle (7)) to achieve steady state. Experimental studies of long-term behaviors are limited by the short lifetime (<20–40 min) of isolated myocytes subjected to periodic pacing (8). In addition, simultaneous monitoring of Na^{+} and Ca^{2+} in subcellular compartments without affecting their balance is difficult, if not impossible (9). Therefore, to describe these phenomena (e.g., ion dynamics in restricted cellular subdomains, rate-dependent long-term ion accumulation), models of the AP and Ca^{2+} cycling that account for dynamic changes of intracellular ion concentrations have emerged (e.g., (10,11)).

Development and application of such physiologically detailed models of cells and tissues is a rapidly growing aspect of research in cardiac electrophysiology, contractility, and arrhythmia. Given the large interspecies differences and greatly varying dynamics in different disease states, it is essential to establish uniform and quantitative criteria for reproducibility, stability, uniqueness, steady state, and conservation laws for all models. Importantly, many simulations involve comparative studies (e.g., diseased compared to normal, comparison of behavior at different rates, comparison between species, etc.). It is imperative that these comparisons are conducted at equivalent physiological states (e.g., steady state). In this article, we develop and present such quantitative criteria.

The repository on www.cellml.com includes >100 different models (12). Using the Hodgkin and Huxley approach (13), contemporary models consist of a large system of nonlinear differential equations, with subsets of the system representing individual ionic currents, specific ion (e.g., Ca^{2+}, Na^{+}, K^{+}, and Cl^{-}) homeostasis, and regulatory pathways (CaMKII, PKA). Given the large scale of the nonlinear system involved, questions were recently raised regarding reproducibility, numerical stability, and uniqueness of model solutions (14–16). The most frequently raised issues include an apparent dependence of the solution on initial conditions, a drift of the state variables (primarily of ion concentrations), and discontinuities in state variables formulation (e.g., the gating variables of the fast sodium current, I_{Na}) (17). Several authors reported that significant modifications were required

Submitted December 11, 2008, and accepted for publication May 19, 2009.

*Correspondence: rudy@wustl.edu

Editor: Michael D. Stern.

0006-3495/09/09/1265/12 $2.00

doi: 10.1016/j.bpj.2009.05.062

before certain single-cell models could simulate AP conduction in multicellular tissue configurations (18,19).

The stability concerns can be resolved by recognizing that the dynamic cell models are realized by a set of differential equations with hidden or explicit algebraic constraints. Such a system, consisting of both differential and algebraic equations, is called a differential-algebraic system or differential-algebraic equations (DAEs). DAEs are widely used for modeling constrained dynamical systems in numerous applications (e.g., mechanical multibody systems, electrical circuit simulations, control theory, fluid dynamics, etc. (20).). In the DAE framework, a consistent set of initial values for state variables and their derivatives must be supplied to insure stability and uniqueness of the solution (20–22). Examples of constraints in cardiac AP cell models (or other excitable cell types) are a conservation relation between membrane voltage and ionic concentrations (16,23) and conservation of total state occupancy in multistate ion channel models (e.g., Markov models). To satisfy a conservation relation between membrane voltage and ionic concentrations, a monophasic stimulus current with K^+ as charge carrier has been used in periodically paced cardiac models (6,24). However, during propagation in the multicellular tissue, the myocyte is subjected to periodic biphasic stimulation, i.e., positive influx of current from the upstream cells is reversed when the myocyte supplies current to downstream cells. Thus, to bridge the gap between single-cell and multicellular model simulations, we tested applications of biphasic stimuli to ventricular myocyte models of the guinea-pig (11,25) and canine (25–27).

The article outline is as follows:

First, uniqueness of model solutions with a consistent set of initial conditions is tested for both quiescent and periodically paced modes.

Second, a conservative biphasic stimulation protocol for a cell is formulated, providing consistent initial conditions for simulations in the multicellular tissue.

Third, a convergence criterion for the steady-state periodic solution is defined, based on the incremental contribution of each ion species to the transmembrane potential during each beat.

Fourth, analytical algebraic expressions are derived to remove singularities in the state variables formulations. Finally, a MATLAB (The MathWorks, Natick, MA) script is developed and implemented for single-cell and cardiac strand simulations.

METHODS

Myocyte models

The theoretical LRd (11) and HRd (26) models of mammalian ventricular AP and Ca^{2+} cycling provide the basis for the simulations. The LRd model is based on guinea-pig data; it includes membrane ion-channel currents, pumps, and exchangers, and accounts for dynamic concentration changes of Na^+, K^+, and Ca^{2+}. The HRd model (Fig. 1) is based on epicardial canine

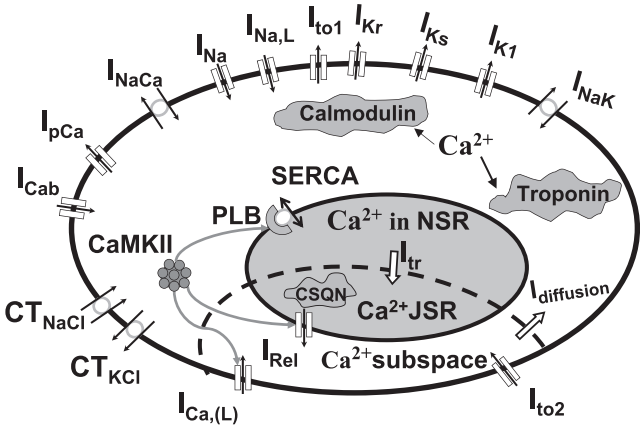

FIGURE 1 Ventricular myocyte model. Symbols are defined in the Supporting Material and in the research section of http://rudylab.wustl.edu.

data (26) and in addition to the above processes includes chloride (Cl^-) homeostasis and CaMKII regulation. Recently, an updated formulation of SR Ca^{2+} release was introduced to the models (25).

Because the LRd model underwent several updates to account for new experimental data since it was first published, we summarize these modifications in the Supporting Material. Models, equations, and code can be found in the research section of http://rudylab.wustl.edu.

Differential-algebraic equation models

A differential-algebraic equation (DAE) is an equation involving an unknown function and its derivatives. It is recognized that a numerical solution that does not satisfy the algebraic constraints (or conservation laws) is unstable and produces drift (20–23). For the sake of clarity and completeness, we briefly introduce definitions related to differential-algebraic equations in the Supporting Material.

Membrane model

According to conservation of charge, the total membrane current density, I_m ($\mu A/cm^2$), which equals the applied stimulus current I_{stim}, can be represented as a sum of capacitive current I_C and the total ionic current I_{ion} (13,29):

$$I_m = I_{stim} = I_C + I_{ion}. \quad (1)$$

In addition, the following relation describes the time-dependent membrane potential V_m (13,29)

$$I_m = I_{stim} = C_{sc}\frac{dV_m}{dt} + I_{ion}, \quad (2)$$

where C_{sc} is the specific membrane capacitance per unit area of membrane (1 $\mu F/cm^2$) (11). Alternatively, V_m can be related to the membrane charge Q as (29)

$$C_{sc}V_m = Q. \quad (3)$$

V_m and the currents obey voltage and current conservation laws and their initial values cannot be arbitrarily selected. Thus, Eqs. 2 and 3 define an electric circuit model that constitutes a DAE system (23) (see Eq. S1.44 and Eq. S1.45 in the Supporting Material). I_{ion} can be written in terms of its ion species,

$$I_{ion} = \sum I_{X,t} = I_{Na,t} + I_{K,t} + I_{Ca,t} + I_{Cl,t}, \quad (4)$$

where $I_{X,t}$ is the sum of all ionic fluxes that carry specific ion X. In dynamic AP models (10,11), state variables are usually intracellular ion

concentrations in different intracellular compartments, thus it is conventional to recast Eq. 3 in terms of concentrations (6,24)

$$C_m V_m = -Q_0 + Q_{stim} + F\sum_X \sum_k v_k z_X [X]_{X,k}, \quad (5)$$

where $F = 96485$ mC/mmol is the Faraday constant, C_m (1.534e-4 μF) is the total myocyte capacitance, $[X]_{X,j}$ is the concentration of ion X of valence z_X in the volume compartment v_k, $Q_{stim} = \int I_{stim} dt$ is the charge provided by the stimulus current, and the parameter Q_0 (nC) accounts for charge contributed by nonspecific, mainly anionic, charged intracellular molecules (e.g., impermeable proteins).

It is clear from Eqs. 2 and 3 that V_m and ion concentrations obey a conservation law, and therefore their initial values cannot be selected arbitrarily (20,21).

For the specific configuration of the HRd model used in this study, conservation relations for V_m (Eq. 3) and its time-derivative (Eq. 2) are expressed using Eq. 5 as

$$\begin{aligned} V_m C_m = {} & F\Big(v_i\Big\{\big[Na^+\big]_i + \big[K^+\big]_i + 2\big[Ca^{2+}\big]_{i,t} - \big[Cl^-\big]_i\Big\} \\ & + 2v_s\big[Ca^{2+}\big]_{s,t} + 2v_j\big[Ca^{2+}\big]_{j,t} + 2v_n\big[Ca^{2+}\big]_n\Big) \\ & + Q_{stim} - Q_0 \end{aligned} \quad (6)$$

and

$$\begin{aligned} C_m \frac{dV_m}{dt} = {} & F\Bigg(v_i\Bigg\{\frac{d\big[Na^+\big]_i}{dt} + \frac{d\big[K^+\big]_i}{dt} + 2\frac{d\big[Ca^{2+}\big]_{i,t}}{dt} \\ & - \frac{d\big[Cl^-\big]_i}{dt}\Bigg\} + 2v_s\frac{d\big[Ca^{2+}\big]_{s,t}}{dt} + 2v_j\frac{d\big[Ca^{2+}\big]_{j,t}}{dt} \\ & + 2v_n\frac{d\big[Ca^{2+}\big]_n}{dt}\Bigg) + I_{stim} \\ = {} & -(I_{Na,t} + I_{K,t} + I_{Ca,t} + I_{Cl,t}) + I_{stim}. \end{aligned} \quad (7)$$

From Eq. 7, it is clear that $I_{stim} = dQ_{stim}/dt$ should account for both V_m and ionic flux changes to satisfy the conservation condition in Eq. 6. Note that, in the LRd formulation, the chloride component $[Cl^-]_i$ and v_s are set to zero.

A procedure for finding the resting initial conditions—the autonomic regime

The specification of initial conditions is quite different for DAEs than for ordinary differential equations (ODEs). For ODEs, a set of initial conditions uniquely determines a solution. For DAEs, it may be difficult to find initial conditions that satisfy all equations, including the constraints. To ensure reproducibility of model results, a set of consistent initial conditions (that satisfy Eqs. 6 and 7 for all state variables and their derivatives) for the DAE system must be provided. Due to the nonlinearity of the model, obtaining resting initial conditions analytically is virtually impossible (20,21,30).

Therefore, numerical procedures are applied as follows: as a first step, state variables that describe ion concentrations and V_m are assigned resting values close to those used in the experiment that corresponds to the particular simulation. Q_0 in Eq. 6 is calculated and kept constant throughout the simulation to insure uniqueness of the solution. Initial values of 1 or 0 are assigned to inactivation or activation gating variables, respectively, which are close to their typical values at resting V_m. To obtain the exact resting state, the model is allowed to run without application of external stimuli (autonomic regime) until all state variables attain steady-state values. These new steady-state values form a consistent set of resting initial conditions. Several models have higher levels of compartmentalization for Ca^{2+} and separate myoplasm and subspace compartments for Na^+ and K^+ (e.g., (31,32)). In these cases, Eq. 6 can be modified using Eq. 5 by adding terms that account for specific ions occupying specific compartments. After these modifications, the proposed procedure can be applied to these aforementioned models also.

In this study, we used the problem-solving environment MATLAB (22), which provides tools for solving DAE (subroutine ODE15s). It should be noted that ODE15s does not require users to recast the equations system in the form of Eq. 6. In addition, users are not required to supply time-derivatives of the vector of initial conditions. If initial conditions and their time derivatives ($\mathbf{y}(0)$ and $\mathbf{y}'(0)$ in Eq. S1.44 and Eq. S1.45) are not consistent, ODE15S treats them as guesses, tries to compute consistent values close to the guesses, and then continues to solve the problem.

Pacing protocols and biphasic stimulation—the paced regime

We use as initial guess resting values computed using the unpaced (autonomic) regime. This approach allows the model to reach steady state at different pacing rates significantly faster. The same biphasic stimulus is used for both guinea-pig and canine models. The positive and negative phases are both square waveforms and the stimulus current (I_{stim}) has a zero mean over a pacing cycle T, i.e., $\int_0^T I_{stim} dt = Q_{stim} = 0$, (there is no net gain of charge). Details are in the Supporting Material.

Removing singularities

In present models, formulation of the gating variables of I_{Na} and $I_{Ca,T}$ (T-type Ca^{2+} current) involve logical expressions that introduce singularities (11). This can cause problems for implementation in a problem solving environment such as MATLAB (22) and for numerical analysis. Here, we replace these discontinuous formulations with functions that have continuous derivatives of all orders (see Supporting Material).

Criterion for steady-state conditions

To evaluate the convergence to steady state of dynamic cardiac cell models, we introduce a criterion that is based on the incremental contribution of each ion species to V_m during each beat. We express the relative contribution to V_m of transient changes in ion concentrations using the relation

$$\begin{aligned} \Delta V_m &= \Delta V_{stim} - \sum_X \Delta V_X \\ &= \Delta V_{Na} + \Delta V_{Ca} + \Delta V_K + \Delta V_{Cl} + \Delta V_{stim}, \end{aligned} \quad (8)$$

where $\Delta V_m = V_m - V_m(t_0)$ is change from end-diastolic value at time t_0, and $\sum_X \Delta V_X$ is the total contribution of all ion species X, (in millivolts) to ΔV_m. $\Delta V_{Na} = V_{Na} - V_{Na}(t_0)$, $\Delta V_K = V_K - V_K(t_0)$, $\Delta V_{Ca} = V_{Ca} - V_{Ca}(t_0)$, and $\Delta V_{Cl} = V_{Cl} - V_{Cl}(t_0)$ are the contributions of these ions to ΔV_m. $V_{Na} = F/C_m v_i[Na^+]_i$, $V_K = F/C_m v_i[K^+]_i$, $V_{Cl} = -F/C_m v_i[Cl^-]_i$, and $V_{Ca} = 2F/C_m(v_i[Ca^{2+}]_{i,t} + v_s[Ca^{2+}]_{s,t} + v_j[Ca^{2+}]_{j,t} + v_n[Ca^{2+}]_n)$ as in Kneller et al. (6).

Steady state is reached when each component of ΔV_{ion} is less than a prescribed δ-value (e.g., $\delta = 0.1$ mV)

$$\Delta V_X < \delta. \quad (9)$$

Alternatively, Eq. 9 can be rewritten for the total amount of each ion species, X, as

$$\Delta X < \delta_C, \quad (10)$$

where $\Delta X = X - X(t_0)$ is the change in the amount of ion from its value at time t_0. In this case the convergence criterion is $\delta_C = \delta/(z_x F/C_m v_i) =$ 6.3e-6 mM for $\delta = 0.1$ mV. This criterion is very sensitive due to the fact that 0.1 mV is equivalent to a nanomolar change of ion concentration.

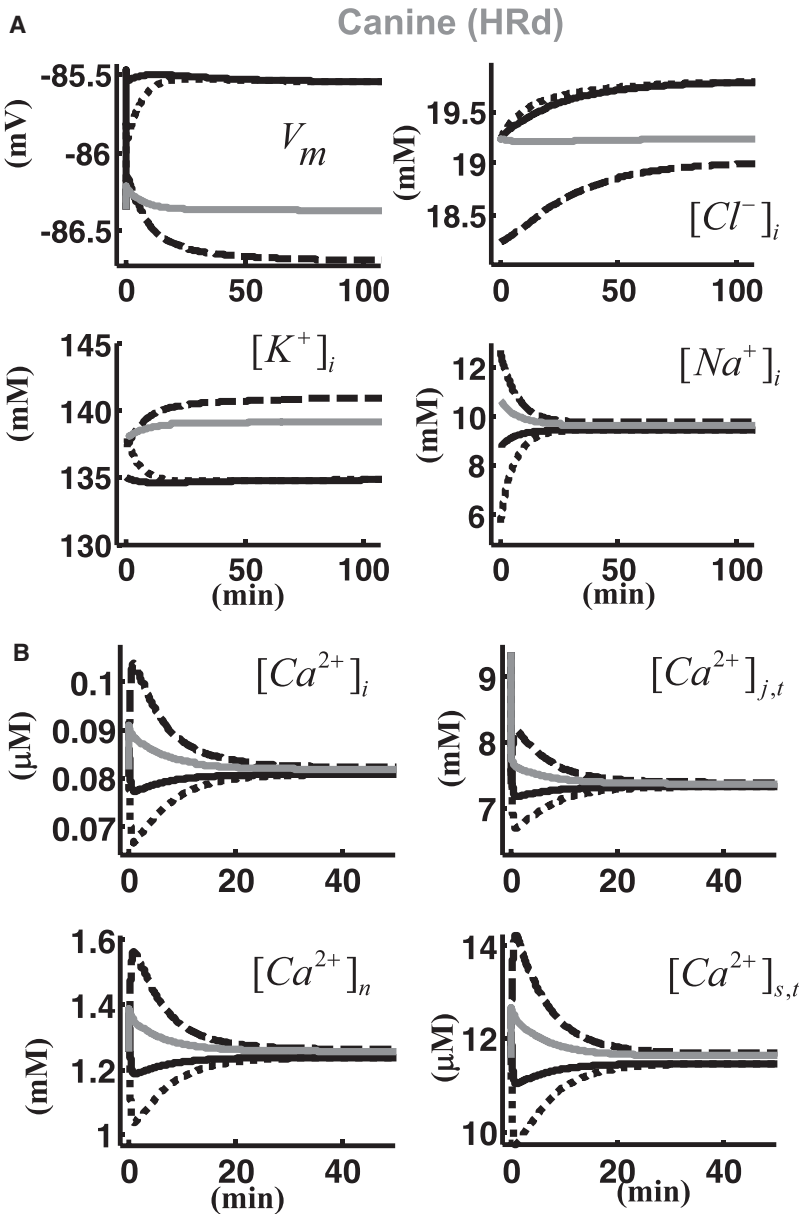

FIGURE 2 Time course to steady state of ion concentrations and membrane potential in a quiescent canine cell model for different initial conditions. (*A*) (*Clockwise*) membrane potential (V_m), myoplasmic concentration of Cl^- ($[Cl^-]_i$), Na^+ ($[Na^+]_i$), and K^+ ($[K^+]_i$). (*B*) (*Clockwise*) myoplasmic concentration of Ca^{2+} ($[Ca^+]_i$), total Ca^{2+} concentrations in junctional SR ($[Ca^+]_{j,t}$), total Ca^{2+} concentration in the subspace ($[Ca^+]_s$), and Ca^{2+} concentration in network SR ($[Ca^+]_n$). (1, *solid line*) $[K^+]_i$ = 135 mM, $[Na^+]_i$ = 8.65 mM, $[Cl^-]_i$ = 19.23 mM; (2, *dashed line*) $[K^+]_i$ = 137 mM $[Na^+]_i$ = 12.65 mM, $[Cl^-]_i$ = 19.23; (3, *dotted line*) $[K^+]_i$ = 138 mM, $[Na^+]_i$ = 5.65 mM, $[Cl^-]_i$ = 19.23; and (4, *shaded line*) $[K^+]_i$ = 138 mM, $[Na^+]_i$ = 10.65 mM, $[Cl^-]_i$ = 18.23 mM; all other initial conditions are the same for all traces.

Note that $\Delta V_{stim} = I_{stim}C_m = 0$ satisfies this criterion for biphasic stimulation. To apply the convergence criterion to other models (e.g., (31,32)), it can be easily modified according to the conservation relation Eq. 5 to add or eliminate state variables or volume compartments. For example, in the LRd formulation the chloride component $[Cl^-]_i$ and v_s are set to zero.

Multicellular fiber model

AP conduction in a cardiac cell strand is computed using the cable equations (13,29) (see Supporting Material for details).

RESULTS

Time course to steady state in the quiescent mode (autonomic regime)

Figs. 2 and 3 show ionic concentrations and membrane potential in quiescent canine and guinea-pig ventricular cell models. Fig. 2 *A* shows time course of (*clockwise*) membrane potential (V_m), myoplasmic concentration of Cl^- ($[Cl^-]_i$), Na^+ ($[Na^+]_i$), and K^+ ($[K^+]_i$) for four different sets of initial ion concentrations in a canine cell:

1. $[K^+]_i$ =135 mM, $[Na^+]_i$=8.65 mM, $[Cl^-]_i$=19.23 mM (*solid line*).
2. $[K^+]_i$ =137 mM, $[Na^+]_i$ = 12.65 mM, $[Cl^-]_i$ = 19.23 (*dashed line*).
3. $[K^+]_i$ = 138 mM, $[Na^+]_i$ = 5.65 mM (*dotted line*), $[Cl^-]_i$ = 19.23.
4. $[K^+]_i$ = 138 mM, $[Na^+]_i$ = 10.65 mM, $[Cl^-]_i$ = 18.23 mM (*shaded line*).

All other state variables have the same initial values for all four traces. Fig. 2 *B* shows (*clockwise*) corresponding myoplasmic concentration of Ca^{2+} ($[Ca^{2+}]_i$), total Ca^{2+}

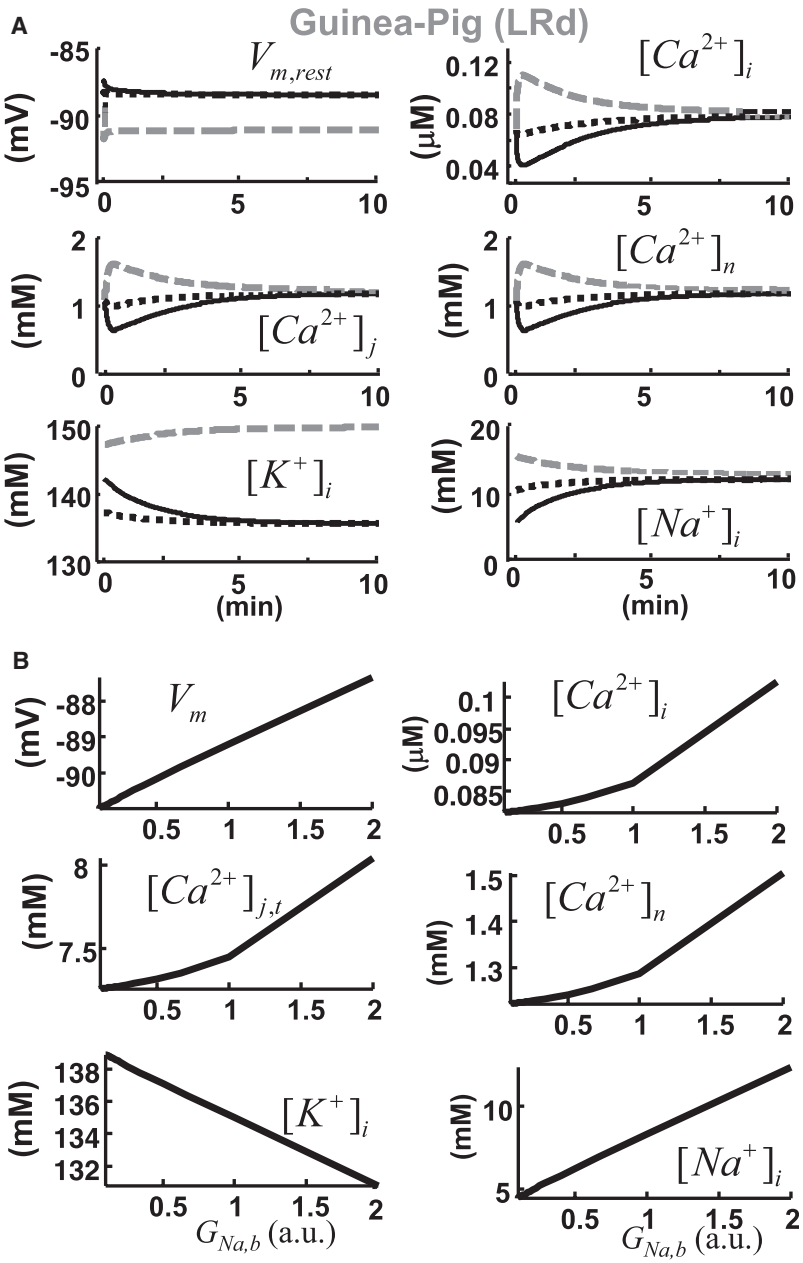

FIGURE 3 (*A*) Ion concentration and membrane potential in a quiescent guinea-pig cell model. Time course starting from assignment of three sets of initial ion concentrations: (1, *solid line*) $[K^+]_i = 142.2$ mM and $[Na^+]_i = 5.6$ mM; (2, *dashed line*) $[K^+]_i = 147.2$ mM and $[Na^+]_i = 15.6$ mM; and (3; *dotted line*) $[K^+]_i = 137.2$ mM and $[Na^+]_i = 10.6$ mM; all other state variables have the same initial values for all traces. (*B*) Effects of sodium background conductance ($G_{Na,b}$) on the steady-state values of ion concentrations and V_m. $G_{Na,b}$ is normalized to its normal value of 0.004 mS/μF.

concentrations in junctional SR ($[Ca^{2+}]_{j,t}$), total Ca^{2+} concentration in the subsarcolemmal subspace ($[Ca^{2+}]_s$), and Ca^{2+} concentration in network SR ($[Ca^{2+}]_n$). After a transient period, steady state is achieved, which depends on the initial concentrations in concordance with the conservation relation Eq. 6. Fig. 3 *A* shows results for the guinea-pig cell model for three sets of initial ionic concentrations:

1. $[K^+]_i = 142.2$ mM and $[Na^+]_i = 5.6$ mM (*solid line*).
2. $[K^+]_i = 147.2$ mM and $[Na^+]_i = 15.6$ mM (*dashed line*).
3. $[K^+]_i = 137.2$ mM and $[Na^+]_i = 10.6$ mM (*dotted line*).

All other state variables have the same initial values for all three traces. The simulations show that Ca^{2+} and Na^+ homeostasis is maintained, i.e., the steady-state concentration reached by each ion is the same for the different sets of initial conditions. This property is conferred by the Ca^{2+} and Na^+ background currents that counterbalance other Ca^{2+} and Na^+ fluxes at the resting V_m (11). The change in $[K^+]_i$ is counterbalanced by the change in V_m and $[Cl^-]_i$. The LRd model achieves steady state in <5 min, faster than the HRd model (20 min) after a similar change in initial ionic concentrations within the physiological range. In both models, V_m reaches steady state first, followed by Ca^{2+} and other ionic concentrations; Cl^- reaches steady state last in the HRd model.

Sets 1 and 3 of initial conditions (*solid* and *dotted black lines*) produce identical resting steady-state values in both models. When sets of initial conditions result in exactly the

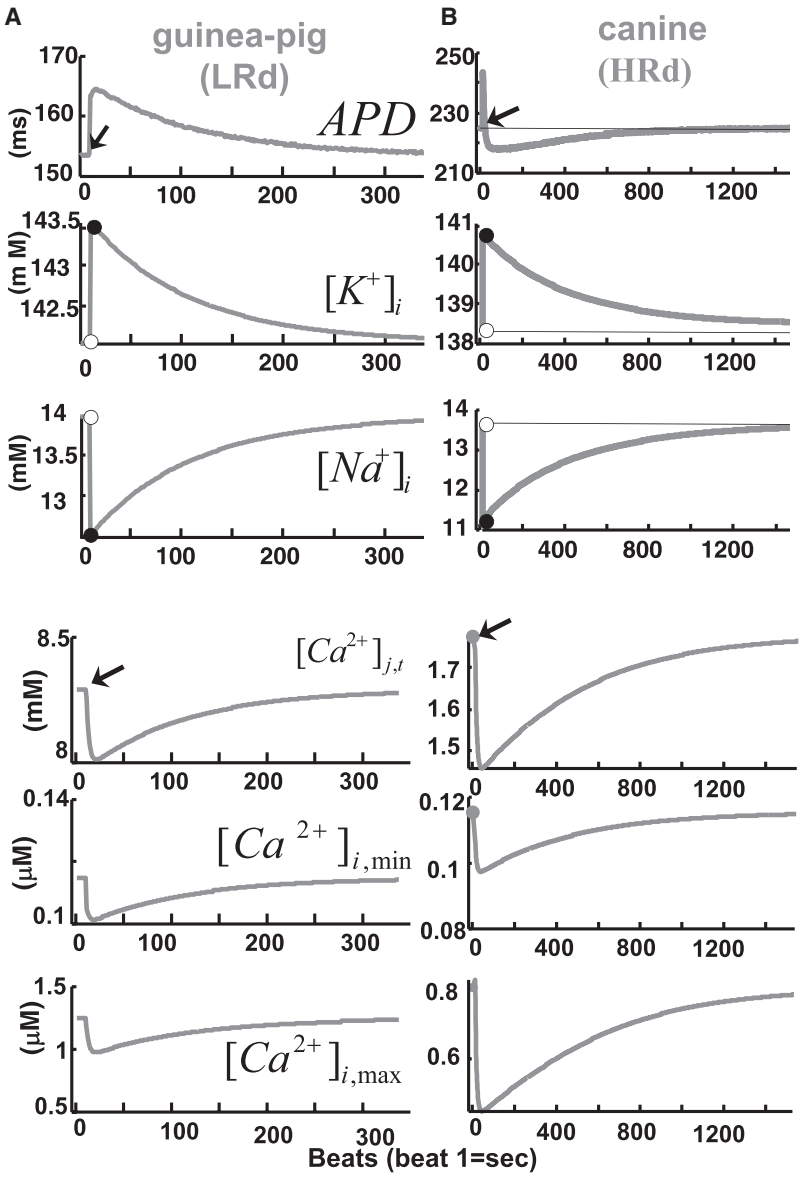

FIGURE 4 Dynamic transient response of guinea pig (*A*) and canine (*B*) cell models to perturbations of ion concentrations from a dynamic steady state during pacing at 1 Hz. $[K^+]_i$ was increased while $[Na^+]_i$ was decreased by 2 mM at the 10th beat (*arrow*); for this perturbation, Eq. 6 is conserved. (*Top* to *bottom*) APD_{90}, total end-diastolic $[Ca^{2+}]_{j,t}$, minimum $[Ca^{2+}]_i$ in myoplasm $[Ca^{2+}]_{i,min}$, and maximum $[Ca^{2+}]_i$ in myoplasm $[Ca^{2+}]_{i,max}$. All concentrations recovered the same values they attained before the perturbation (see text for details).

same value of Q_0 in Eq. 7, all state variables reach the same steady-state values in both models (*dashed* and *solid lines*) regardless of the initial conditions. Since in a conservative system resting ion concentrations cannot be specified a priori and must be found by solving Eq. 2 in conjunction with Eq. 3, it is desirable to identify model parameters that can be used to modify resting initial concentrations according to experimental values. Fig. 3 *B* shows the effect of the sodium background conductance ($\overline{G}_{Na,b}$) on the steady-state values of ionic concentrations and V_m in a quiescent guinea-pig cell. $\overline{G}_{Na,b}$ is normalized to its normal value of 0.004 μA/μF. Using $\overline{G}_{Na,b}$ as a parameter allows us to modify internal $[Na^+]_i$ from 5 to 12 mM while maintaining all other state variables within the physiological range.

We evaluate the stability of the steady-state solutions obtained above by perturbations consistent with the conservation relation in Eq. 6; results are shown in Fig. S1. All state variables (ion concentrations) return to their initial values regardless of the amplitude and type of perturbation.

Periodically paced cells (paced regime)

Starting from quiescent steady-state values, both HRd and LRd models were paced with a current stimulus as in Eq. S1.47 until the steady state defined in Eq. 8 was reached. Then, the end-diastolic values of $[K^+]_i$ and $[Na^+]_i$ were changed and pacing was resumed. Fig. 4 shows LRd (*A*) and HRd (*B*) model responses to sudden change of ionic concentrations. Both models were paced until steady state at 1Hz, and at the following 10th beat (*arrow*) $[K^+]_i$ was increased while $[Na^+]_i$ was decreased by 2 mM. Pacing continued at the same rate until a new steady state was reached. The new steady-state values were exactly the same as before the perturbation. Each panel shows (*top* to

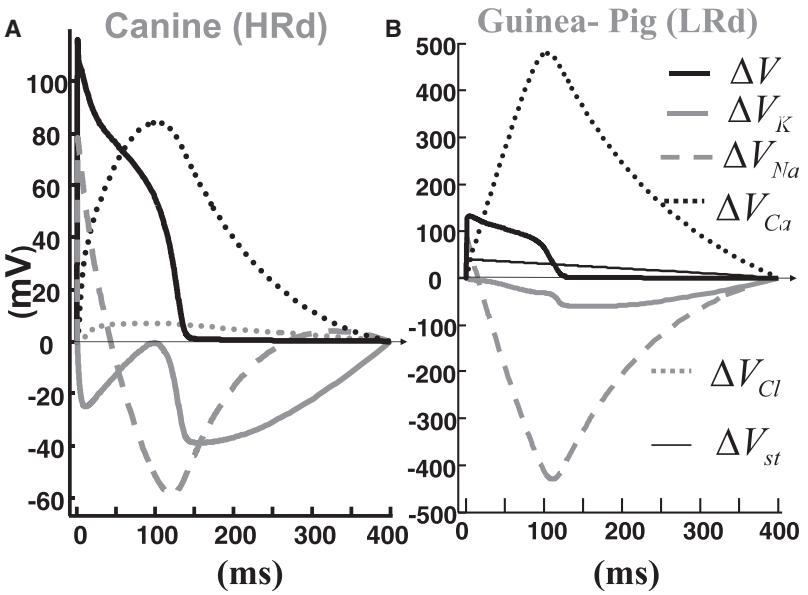

FIGURE 5 Ionic balance during a cardiac cycle in the cell model at periodic steady state during pacing at CL = 400 ms. (*A*) Canine and (*B*) guinea pig. ΔV_{Na} (*dashed gray*), ΔV_{Ca} (*dotted black*), ΔV_K (*solid gray*), and ΔV_{Cl} (*dotted gray*) are contributions of Na^+, Ca^{2+}, K^+, and Cl^- ions, respectively, to the membrane voltage change (ΔV_m; *solid black*) as defined in Eq. 8.

bottom) APD calculated at 90% of repolarization (APD_{90}), $[K^+]_i$, $[Na^+]_i$, total end-diastolic $[Ca^{2+}]_{j,t}$, minimum$[Ca^{2+}]_i$ in myoplasm ($[Ca^{2+}]_{i,min}$), and maximum $[Ca^{2+}]_i$ in myoplasm ($[Ca^{2+}]_{i,max}$). Solid circles show $[K^+]_i$ and $[Na^+]_i$ just after the perturbation from their dynamic steady-state values (*open circles*). Steady-state values are rate-dependent; APD_{90} approaches steady-state values faster than the Ca^{2+} transient and the other ion concentrations. Note that a sudden decrease in $[Na^+]_i$ results in a transient APD prolongation and a decrease of the intracellular Ca^{2+} content and peak $[Ca^{2+}]_i$ transient. In LRd, the APD increases when $[Na^+]_i$ decreases. In HRd, the APD response is triphasic, with initial lengthening followed by shortening with overshoot (Fig. 4 *B*, *top*). The Ca^{2+} subsystem responds similarly in both models with transitory decrease of the Ca^{2+} content in SR and myoplasm (*right panels*). Note that in paced regime LRd recovers from perturbations in <5 min, faster than HRd (30 min).

Application of the steady-state criterion Eq. 8 is illustrated in Fig. 5. Results in Fig. 5 *A* show ionic balances during a cardiac cycle (CL = 400 ms) in the HRd model. Fig. 5 *B* shows similar data for the guinea-pig model. Note that the HRd model includes a Cl^--dependent component that is not included in the LRd model. ΔV_{Na} (*dashed gray*), ΔV_{Ca} (*dotted black*), ΔV_{Cl} (*dotted gray*), and ΔV_K (*solid gray*), are the contributions of Na^+, Ca^{2+}, Cl^-, and K^+ ions, respectively, to membrane voltage change ΔV_m (*solid black*). Note that the HRd and LRd model cells do not gain or lose any ions over one beat, verifying that the periodic condition Eq. S1.46 is completely satisfied.

Effect of stimulus assignment on ionic homeostasis and dynamic properties

In Fig. 6, both cells are paced with a traditional monophasic stimulus carried by K^+ (*shaded lines*) and a biphasic stimulus that carries zero charge over one beat (*solid lines*). All other parameters and initial conditions are identical in these simulations. Fig. 6 *A* shows (clockwise) $[Na^+]_i$, $[K^+]_i$, APD_{90}, and end-diastolic V_m ($V_{m,rest}$) as function of pacing rate. Both protocols lead to identical results at the range of pacing frequencies from 0.125 to 2 Hz. However, the $[K^+]_i$ and $[Na^+]_i$ curves reach saturation at frequencies higher than 4 Hz in the cell paced with the monophasic stimulus. In contrast, under biphasic stimulation, $[K^+]_i$ continues to decrease in accordance with conservation relation Eq. 6. The difference between monophasic and biphasic stimulation reaches 6 mM at a frequency of 6 Hz, where the monophasic-driven model loses its one-to-one capture. $V_{m,rest}$ is increased as a function of pacing rate in both models, in accordance with experimental findings (4,7). APD_{90} of the monophasic-driven cell is significantly longer at pacing rates above 1 Hz relative to that of the biphasic-driven cell. The onset frequency of APD alternans (3.3 Hz) in the canine model is similar for both stimulation protocols. However, the alternans amplitude is significantly greater in the canine cell driven by K^+ monophasic stimulation. APD prolongation prevents one-to-one capture at rate above 6 Hz in the monophasically paced cell because the diastolic interval after the long APD approaches zero.

In the guinea pig (Fig. 6 *B*), biphasic stimulation leads to increase of $[Na^+]_i$ and decrease of $[K^+]_i$ by 2 mM at fast rates (>3 Hz), relative to the monophasic-driven cell. Cellular Ca^{2+} content is similar for both stimulations (not shown). $V_{m,rest}$ is higher by 2 mV in the monophasic K^+-driven cell, in accordance with experiments (4,7), and APD is longer by 10 ms.

In summary, pacing with a monophasic stimulus carried by K^+ leads to overestimation of $[K^+]_i$ and underestimation of $[Na^+]_i$ at fast rate (>3 Hz) in both cells, relative to biphasic stimulation. This stimulus effect is larger in the

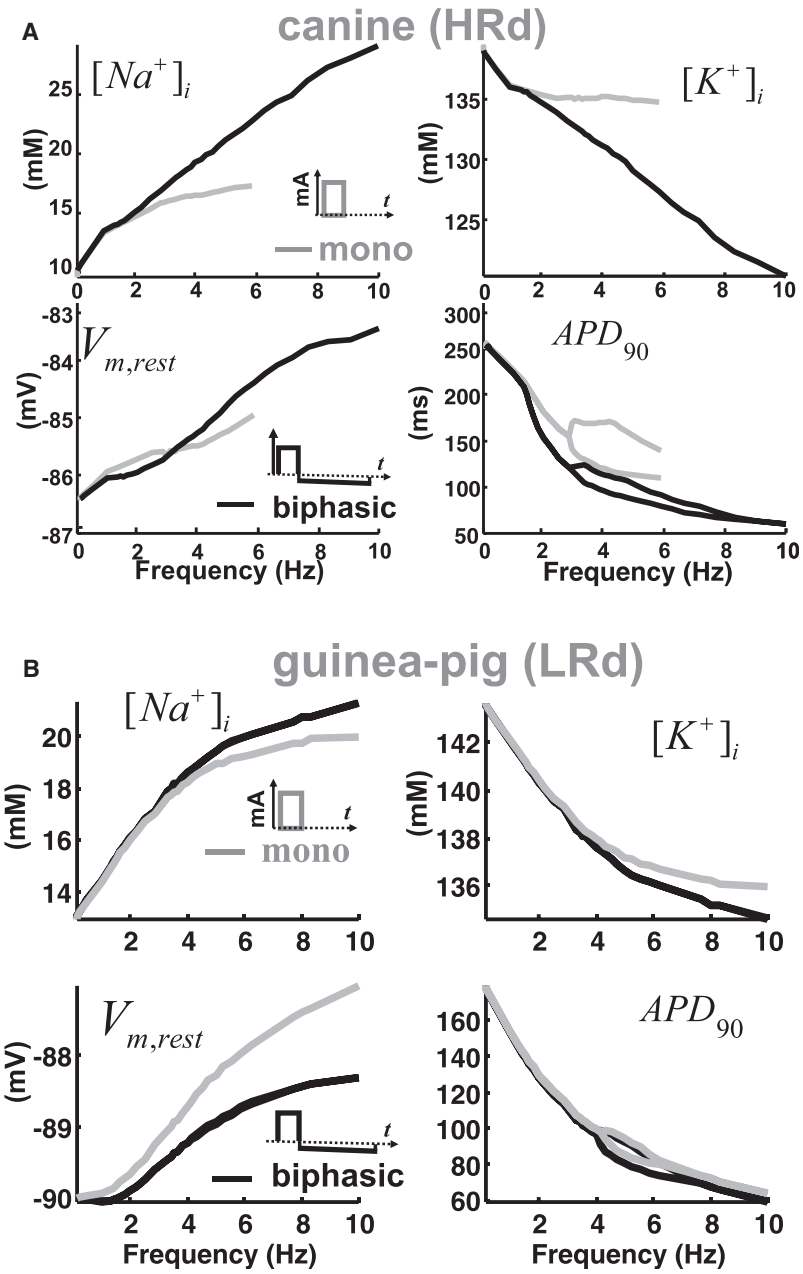

FIGURE 6 Rate dependence during pacing by monophasic (*shaded*) and biphasic (*solid*) stimulus current. (*A*) Canine and (*B*) guinea pig. Steady-state end-diastolic values of $[Na^+]_i$, $[K^+]_i$, $V_{m,rest}$, and APD_{90} are shown. Note bifurcation of APD_{90} into alternans mode at fast rate (>3 Hz).

canine than in the guinea-pig cell; it does not exist in the beating heart, where cells are exposed to biphasic stimulation. In addition, monophasic protocols can overestimate APD relative to biphasic stimulation during AP propagation.

Axial current and multicellular strand simulations (conduction regime)

Fig. 7 shows simulated propagating AP (4 consecutive beats) in a 1-cm-long cardiac strand paced at 5 Hz . Fig. 7, *A* and *B*, show results in the LRd and HRd models, respectively. Fig. S2 in the Supporting Material shows axial current and its running integral (charge) for cells $n = 25$ and 85 for the cardiac strand with the HRd model. Results demonstrate the correspondence of the excitatory charge experienced by a cell in the fiber during propagation to that experienced by a single cell during biphasic simulation; in both cases the excitatory current has a zero mean over the excitation cycle.

Increase of D (diffusion coefficient; see the Supporting Material) by a factor of 4 in Fig. S2 increases conduction velocity from 25 cm/s to 50 cm/s, which correlates well with the experimentally measured velocity in well coupled (normal) cardiac tissue. Conduction velocity is estimated using the time difference between positive peaks of I_{axial} at different nodes. Note that increase of D by a factor of 4 results in a twofold increase in velocity, as expected by the theoretical square-root relationship.

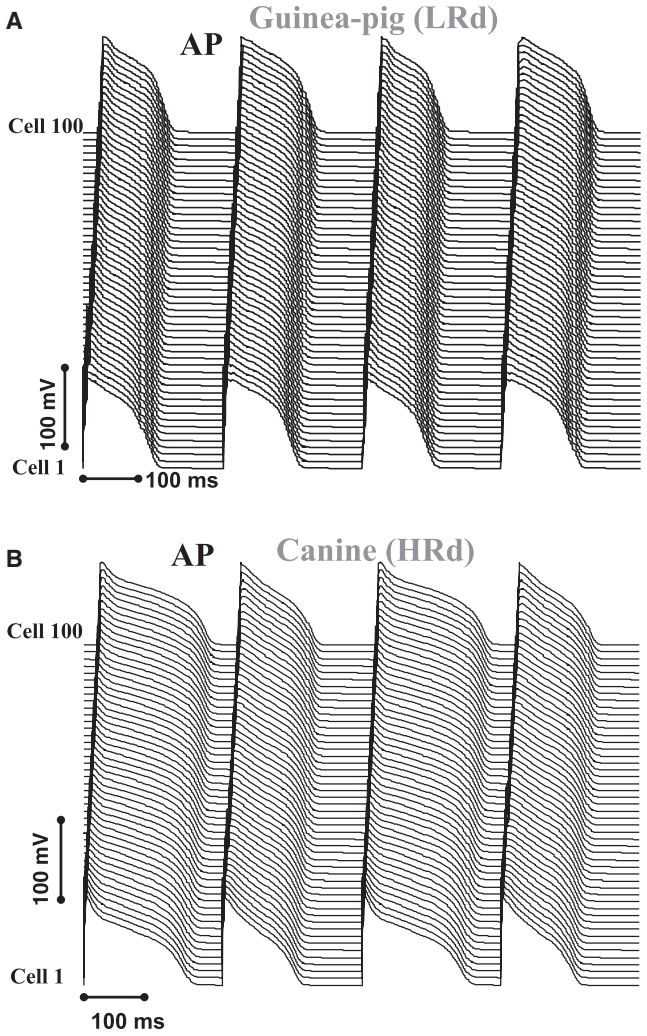

FIGURE 7 AP propagation in one-dimensional fiber. (*A*) Guinea pig. (*B*) Canine. Both models were simulated with the same geometrical and electrical parameters. Diffusion coefficient $D = 0.000856\ \text{cm}^2/\text{ms}$ results in conduction velocity of 46 cm/s in both models. At the simulated pacing frequency of 5 Hz (CL = 200 ms), AP exhibits alternans in both models. APD alternans in the canine (APD_{long} = 160 ms; APD_{short} = 130 ms) is of greater amplitude than in the guinea pig (APD_{long} = 90 ms; APD_{short} = 80 ms).

DISCUSSION

In this study, we found that ventricular myocyte models of the guinea-pig and canine AP and Ca^{2+} cycling reach unique steady-state solutions in a quiescent mode and during periodic pacing. Recognizing that these models are represented by a system of DAEs, consistency with an algebraic (conservation constraints) set of initial conditions is mandatory for achieving unique steady-state solutions. We provide a numerical procedure for obtaining such a set of initial conditions using the problem-solving environment MATLAB. We also demonstrate the large benefit of using the entire set of steady-state values computed for a single cell under biphasic stimulation as an initial guess for multicellular simulations of AP propagation.

A cell membrane behaves as a capacitor, and any ion that crosses the cell membrane contributes to V_m; reciprocally, any change in V_m must be accounted for by transmembrane ion fluxes (6,24). This implies that the cell is a conservative system and the total amount of charge (ions) is conserved. This includes charge carried by mobile ions (e.g., K^+, N^+, Ca^{2+}) that are explicitly accounted for by the model equations, and charge (e.g., carried by intracellular proteins) represented by the parameter Q_0 in Eq. 6. Simulations that start with different total amounts of ions (sum of all ion species) evolve to different steady-state solutions (ion concentrations and V_m). However, if the total ion concentration (sum of all ion species) is conserved between simulations (i.e., simulations start with the same total amounts of ions), then the models evolve to the same steady-state solution in both quiescent and paced modes regardless of the initial concentration of each ion species, as shown in this article (Figs. 2 and 3). The conservation law implies also that only a subset (n-1 out of n) of the terms in Eq. 6 can be controlled and that the remaining ion species or V_m will be dependent through the conservation relation.

Importance of steady state

There are various informal methods for evaluating the convergence to steady state of dynamic cardiac cell models. It is not an easy task, because these models consist of a large system of state variables that have very different steady-state values (e.g., 140 mM for K^+, and 0.1 μM for Ca^{2+}) and time constants (e.g., 0.2 ms for Na^+ channel activation gate and 30 min for intracellular Na^+ accumulation).

Examples of steady-state analysis include methods that are based on beat-to-beat variation of APD (17) or peak Ca^{2+} transient (31). These methods overlook ionic processes that reach steady state with a much longer time course. There are also other ad hoc methods that simply ''eyeball'' the saturation of long-term ionic transients (6,24). These approaches lack an objective quantitative criterion for convergence to steady state, which can be implemented in the code to trace the convergence process automatically.

We previously defined steady state as the state when all variables show less than a predefined percent variability (e.g., $< 0.1\%$) over a certain period of time (e.g., 1 min) (25). However, this criterion did not take into account dependence of the convergence rate on the rate of periodic pacing and the relative contribution of the different state variables to variations of APD and the Ca^{2+} transient. In addition, implementation of such criterion for a system with a large number of state variables becomes cumbersome.

In this study, we introduce a criterion that is based on the incremental contribution of each ion species to the membrane voltage during each beat. This precise criterion allows quantitative evaluation of model convergence to the steady state. We show that this criterion is more reliable than those based on APD only (Fig. 4). It is easy to implement because only

values of several state variables are used (Eq. 8) and no detection of peaks or zero crossings of the state variables and their derivatives is required, as for the APD-based criterion. In addition, it can be easily modified according to the conservation relation Eq. 5 to add or eliminate state variables. This criterion is especially important at fast pacing rate, when the solution involves bifurcation (i.e., a major change in the behavior of the solution in response to a small change of a parameter) such as the onset of AP alternans (25,33), spontaneous SR Ca^{2+} release (34), etc.

Steady state is also essential for conducting models comparisons. Comparing properties (e.g., APD, Ca^{2+} transient, ion concentrations, etc.) between different cell models must be conducted at equivalent physiological states for all models, of which steady-state is unambiguously defined using the criterion presented here. The common practice (e.g., (19,35)) of comparing solutions of different models at a prescribed time (e.g., at a certain simulation time or number of beats after beginning of pacing) can be very misleading, as different models reach steady state with a different time course and could be at very different physiological states at the time of comparison. An adequate comparison between different dynamic models and validation against experimental data should include:

1. The same set of parameter values (e.g., extracellular ionic concentrations);
2. A consistent set of initial conditions for state variables (V_m, intracellular ion concentrations);
3. The same protocol (e.g., periodic pacing at steady state, or nonperiodic transients such as during restitution);
4. Application of a consistent steady-state criterion.

Time course to steady state

Results in this article are shown for HRd (dog) and LRd (guinea-pig) models, to demonstrate model (species) independence of the studied phenomenon. These two species differ in their AP morphology due to differences in ion channel expression levels and kinetic properties. Specifically, the repolarizing currents I_{Ks} and I_{Kr} are significantly smaller (>5 times) in the dog than in the guinea-pig myocyte (26) and so is the L-type Ca^{2+} current during the plateau phase of the AP. Thus, it is not surprising that these cells exhibit different transients in response to perturbations. Current density of the Na^+/K^+ pump in the HRd model is 0.62 $\mu A/\mu F$, which corresponds well with experimental data from canine ventricle epicardial myocytes (36).

The LRd model in the quiescent regime achieves steady state in 5 min, faster than the HRd model (25 min) after a comparable change in initial ionic concentrations within the physiological range. Similar results for the paced regime are shown in Fig. 4. In Fig. 4 *B*, canine APD achieves steady state after 10 min and the corresponding ion concentrations after 25–30 min. This time course is consistent with experimental results for canine atria preparation (6). The faster guinea-pig model response to perturbations can be explained by larger ionic shifts during a single cardiac cycle (Fig. 5). We showed previously that this difference has an important implication in the coupling between Ca^{2+} cycling and AP duration in the context of Ca^{2+} alternans (25).

In both guinea-pig and canine models, V_m reaches steady state first, followed by intracellular Ca^{2+} and other ionic concentrations; Cl^- reaches steady-state last in the canine model, consistent with a previous study in canine atrial cells (6). The time course to reach steady state is within the physiological range (3,4,6). APD reaches steady state faster than most ionic concentrations. This underlies the deficiency of the APD-based convergence criterion for dynamic models of the cardiac AP. It should be noted that in the periodically paced mode, both models return to their original steady-state values after perturbations that are consistent with the conservation constraints (Fig. 5).

Rate dependence of ionic balance during biphasic stimulation

APD rate-adaptation curves generated by the guinea-pig and canine models show significant dependence on the stimulus current assignment (Fig. 6). Previous studies showed that assignment of the stimulus charge to any of the intracellular ion species eliminates drift in the model solution (6,24). Using K^+ ions as the stimulus carrier was found to be most appropriate, due to the small perturbation of the large $[K^+]_i$ (140 mM)) by the small stimulus charge (6). Here we showed that although this approach is adequate at slow-to-moderate pacing rates (<2 Hz), using K^+ as charge carrier can significantly underestimate intracellular Na^+ accumulation at fast rates. Several studies (6,17) reported that up to 5 mM K^+ accumulates in the myoplasm at fast rate due to stimulus assignment. This seems a minor gain relative to resting $[K^+]_i$, which is ~140 mM. However, due to the conservation relation, Eq. 6, $[Na^+]_i$ (and possibly other cations) is reduced on the background of a much smaller intracellular concentration. Such significant percent change affects the Ca^{2+} transient and AP morphology. This stimulus effect is larger in the canine than in the guinea-pig cell due to differences in ionic flux balances during the cardiac cycle. As stated above, these effects are not present in cardiac tissue under physiological conditions where myocytes are exposed to biphasic stimulation, serving first as a sink for upstream cells, then a source for downstream cells.

The depolarization trend of the end-diastolic membrane potential ($V_{m,rest}$) at fast rate is consistent with experimental data (4). Intracellular sodium accumulation is consistent with rate-dependent data presented in Mills et al. (9) (16 mM at 2.5 Hz). Steady-state values at pacing frequencies above 5 Hz reach higher values, which may be relevant during tachycardia and fibrillation when frequency can reach these values.

AP propagation in cardiac strand

The most time-consuming step in propagation simulations is finding the steady-state solution for each parameter space. In the example of Fig. 7, we use as initial guess values computed using the single-cell model driven by a biphasic stimulus at 5 Hz. This approach allows us to drive the cardiac strand model into the alternans mode immediately after the onset of stimulation. We expect this approach to greatly accelerate the convergence of one- and two-dimensional simulations.

Results in Fig. 7 and Fig. S2 further validate our assumption that in the tissue, myocytes are subjected to periodic biphasic stimulation, i.e., positive influx of current from upstream cells is reversed when myocytes supply current to downstream cells. Several authors reported that significant modifications were required before certain single cell models could be incorporated successfully to simulate AP conduction in multicellular configurations (18,19). This observation is not surprising, because models of AP and Ca^{2+} cycling are fitted to data from isolated single-cell and single-channel experiments, removed from the electrophysiological environment where cardiac cells normally operate. Electrotonic effects of surrounding tissue (both excitable and passive) can change AP morphology substantially and consequently affect Ca^{+} dynamics. The most widely used approach to overcame electrotonic effects is to augment conductances of the fast Na^{+} and L-type Ca^{+} currents (e.g., (18)). These modifications, although allowing us to simulate AP propagation, affect the rate-dependent Na^{+} -Ca^{2+} balance. In this study, after increasing I_{Na} conductance by 40%, the single-cell model was paced to steady-state by biphasic stimulus at different rates to insure that accumulation of Na^{+} and Ca^{2+} was in the physiological range.

To simplify single cell models, dynamic changes of ionic concentrations were eliminated from the models (14,15), keeping their values constant (e.g., K^{+} in (17)), or using empirical relations between stimulation rate and intracellular concentrations (e.g., Na^{+} in (33)). In addition, several studies advocated the use of reduced (e.g., without Ca^{2+} cycling) models in multicellular simulations to decrease computation (35,37). This reductionist approach limits greatly the validity of these models and their applicability to various pathological conditions in the context of cardiac arrhythmia (34). Inclusion of dynamic changes of intracellular ionic concentrations requires a long computing time to reach steady state, which is difficult in many two- and three-dimensional simulations. We overcome this difficulty by initializing the multicellular model with rate-dependent steady-state values obtained from single-cell simulations under biphasic stimulation, a condition that mimics cell excitation in the multicellular tissue during AP propagation.

A computational note

The cardiac cell model is a highly nonlinear dynamic system exhibiting fast and slow changing modes; it can be classified as a typical stiff system of equations. Computational considerations are discussed briefly in the Supporting Material.

SUPPORTING MATERIAL

Two figures and one table are available at http://www.biophysj.org/biophysj/supplemental/S0006-3495(09)01159-X.

We thank members of the Rudy Lab: K. Decker, N. Gaur, T. O'Hara, Dr. A. Nekouzadeh, J. Heijman, and Dr. J. Silva for helpful discussions. Y. Rudy is the Fred Saigh Distinguished Professor at Washington University.

This research was supported by the National Institutes of Health-National Heart, Lung and Blood Institute merit award No. R37-HL 33343 and grant No. RO1-HL 49054, and by Fondation Leducq Award to the Alliance for CaMK Signaling in Heart Disease (to Y. Rudy).

REFERENCES

1. ter Keurs, H. E. D. J., and P. A. Boyden. 2007. Calcium and arrhythmogenesis. *Physiol. Rev.* 87:457–506.
2. Bers, D. N. 2001. Excitation-Contraction Coupling and Cardiac Contractile Force. Kluwer Academic Publishers, Dordrecht, The Netherlands.
3. Eisner, D. A. 1990. Intracellular sodium in cardiac-muscle—effects on contraction. *Exp. Physiol.* 75:437–457.
4. Attwell, D., I. Cohen, and D. A. Eisner. 1981. The effects of heart rate on the action potential of guinea-pig and human ventricular muscle. *J. Physiol.* 313:439–461.
5. Sejersted, O. M., and G. Sjogaard. 2000. Dynamics and consequences of potassium shifts in skeletal muscle and heart during exercise. *Physiol. Rev.* 80:1411–1481.
6. Kneller, J., R. J. Ramirez, D. Chartier, M. Courtemanche, and S. Nattel. 2002. Time-dependent transients in an ionically based mathematical model of the canine atrial action potential. *Am. J. Physiol. Heart Circ. Physiol.* 282:H1437–H1451.
7. Davidenko, J. M., R. J. Levi, G. Maid, M. Elizari, and M. Rosenbaum. 1990. Rate dependence and supernormality in excitability of guinea pig papillary muscle. *Am. J. Physiol. Heart Circ. Physiol.* 259:H290–H299.
8. Tolkacheva, E. G., J. M. B. Anumonwo, and J. Jalife. 2006. Action potential duration restitution portraits of mammalian ventricular myocytes: role of calcium current. *Biophys. J.* 91:2735–2745.
9. Mills, G. D., D. M. Harris, X. W. Chen, and S. R. Houser. 2007. Intracellular sodium determines frequency-dependent alterations in contractility in hypertrophied feline ventricular myocytes. *Am. J. Physiol. Heart Circ. Physiol.* 292:H1129–H1138.
10. DiFrancesco, D., and D. Noble. 1985. A model of cardiac electrical activity incorporating ionic pumps and concentration changes. *Philos. Trans. R. Soc. Lond. Biol.* 307:H290–H299.
11. Luo, C. H., and Y. Rudy. 1994. A dynamic model of the cardiac ventricular action potential. I. Simulations of ionic currents and concentration changes. *Circ. Res.* 74:1071–1096.
12. Hunter, P. J., E. J. Crampin, and P. M. F. Nielsen. 2008. Bioinformatics, multiscale modeling and the IUPS Physiome Project. *Brief. Bioinform.* 9:333–343.
13. Hodgkin, A. L., and A. F. Huxley. 1952. A quantitative description of membrane current and its application to conduction and excitation in nerve. *J. Physiol.* 117:500–544.
14. Wilders, R. 2007. Computer modeling of the sinoatrial node. *Med. Biol. Eng. Comput.* 45:189–207.
15. Krogh-Madsen, T., P. Schaffer, A. D. Skriver, L. K. Taylor, B. P. B. Koidl, et al. 2005. An ionic model for rhythmic activity in small clusters of embryonic chick ventricular cells. *Am. J. Physiol. Heart Circ. Physiol.* 289:H398–H413.

16. Fraser, J. A., and C. L. H. Huang. 2007. Quantitative techniques for steady-state calculation and dynamic integrated modeling of membrane potential and intracellular ion concentrations. *Prog. Biophys. Mol. Biol.* 94:336–372.

17. Kurata, Y., I. Hisatome, H. Matsuda, and T. Shibamoto. 2005. Dynamical mechanisms of pacemaker generation in IK1-downregulated human ventricular myocytes: insights from bifurcation analyses of a mathematical model. *Biophys. J.* 89:2865–2887.

18. Garny, A., P. Kohl, P. J. Hunter, M. R. Boyett, and D. Noble. 2003. One-dimensional rabbit sinoatrial node models: benefits and limitations. *J. Cardiol. Electrophys.* 14:S121–S132.

19. Cherry, E. M., and F. H. Fenton. 2004. Suppression of alternans and conduction blocks despite APD restitution: electrotonic, memory and conduction velocity effects. *Am. J. Physiol. Heart Circ. Physiol.* 286:H2332–H2341.

20. Kunkel, P., and V. Mehrmann. 2006. Differential-Algebraic Equations. European Mathematical Society, Zurich, Switzerland.

21. Brown, P. N., A. C. Hindmarsh, and L. R. Petzold. 1987. Consistent initial condition calculation for differential-algebraic systems. *SIAM J. Sci. Comput.* 111:427–430.

22. Shampine, L. F., M. W. Reichelt, and J. A. Kierzenka. 1999. Solving index-1 DAEs in MATLAB and Simulink. *SIAM Rev.* 41:538–552.

23. Varghese, A., and G. R. Sell. 1989. A conservation principle and its effect on the formulation of Na^+/Ca^{2+} exchanger current in cardiac cells. *J. Theor. Biol.* 7:33–40.

24. Hund, T. J., J. P. Kucera, N. F. Otani, and Y. Rudy. 2001. Ionic charge conservation and long-term steady state in the Luo-Rudy dynamic cell model. *Biophys. J.* 81:3324–3331.

25. Livshitz, L. M., and Y. Rudy. 2007. Regulation of Ca^{2+} and electrical alternans in cardiac myocytes: role of CAMKII and repolarizing currents. *Am. J. Physiol. Heart Circ. Physiol.* 292:H2854–H2866.

26. Hund, T. J., and Y. Rudy. 2004. Rate dependence and regulation of action potential and calcium transient in a canine cardiac ventricular cell model. *Circulation.* 110:3168–3174.

27. Decker, K. F., J. Heijman, J. R. Silva, T. J. Hund, and Y. Rudy. 2009. Properties and ionic mechanisms of action potential adaptation, restitution and accommodation in canine epicardium. *Am. J. Physiol. Heart Circ. Physiol.* 296:H1017–H1026.

28. Reference deleted in proof.

29. Jack, J. J. B., D. Noble, and R. W. Tsien. 1988. Electric Current Flow in Excitable Cells. Clarendon Press, Oxford, UK.

30. Jacquemet, V. 2007. Steady-state solutions in mathematical models of atrial cell electrophysiology and their stability. *Math. Biosci.* 208: 241–269.

31. Shannon, T. R., F. Wang, J. Puglisi, C. Weber, and D. M. Bers. 2004. A mathematical treatment of integrated Ca^{2+} dynamics within the ventricular myocyte. *Biophys. J.* 87:3351–3371.

32. Faber, G. M., J. Silva, L. Livshitz, and Y. Rudy. 2006. Kinetic properties of the cardiac L-type Ca^{2+} channel and its role in myocyte electrophysiology: a theoretical investigation. *Biophys. J.* 92:1522–1543.

33. Shiferaw, Y., M. A. Watanabe, A. G. J. Weiss, and A. Karma. 2003. Model of intracellular calcium cycling in ventricular myocytes. *Biophys. J.* 85:3666–3686.

34. Maltsev, V. A., T. M. Vinogradova, and E. G. Lakatta. 1994. The emergency of a general theory of the initiation and strength of the heart beat. *J. Pharmacol. Sci.* 100:338–369.

35. Bueno-Orovio, A., E. M. Cherry, and F. H. Fenton. 2008. Minimal model for human ventricular action potentials in tissue. *J. Theor. Biol.* 253:544–560.

36. Gao, J., W. Wang, I. S. Cohen, and R. Mathias. 2005. Transmural gradients in Na/K pump activity and $[Na^+]_i$ in canine ventricle. *Biophys. J.* 89:1700–1709.

37. ten Tusscher, K. H., and A. V. Panfilov. 2006. Cell model for efficient simulation of wave propagation in human ventricular tissue under normal and pathological conditions. *Phys. Med. Biol.* 51:6141–6156.